Supporting Online Material for

High Gamma Power Is Phase-Locked to Theta Oscillations in Human Neocortex

R. T. Canolty,* E. Edwards, S. S. Dalal, M. Soltani, S. S. Nagarajan,
H. E. Kirsch, M. S. Berger, N. M. Barbaro, R. T. Knight

*To whom correspondence should be addressed. E-mail: rcanolty@berkeley.edu

This PDF file includes:

Materials and Methods
SOM Text
Figs. S1 to S8
References

Supporting Online Material

MATERIALS AND METHODS

PARTICIPANTS

The five patients (all female, age range 24-45 years) participating in this study were undergoing surgical treatment for intractable epilepsy. Patients underwent a craniotomy for subdural implantation of an electrode grid and strip/depth electrodes followed by approximately one week of continuous monitoring of the electrocorticogram (ECoG). This monitoring was done in order to localize 1) the seizure focus for later resection, and 2) critical language and motor areas to be avoided during resective surgery. Grid placement was determined entirely by clinical necessity and was over the left frontotemporal region in all patients. See CLINICAL INFORMATION AND ADDITIONAL TESTS for patient details.

Consenting patients participated in the research study during the week of ECoG monitoring. The study protocol, approved by the UCSF and UC Berkeley Committees on Human Research, did not interfere with the ECoG recordings made for clinical purposes, and presented minimal risk to the participating subjects. Several sensory, motor, and cognitive tasks were performed by the subjects while the ongoing ECoG was recorded continuously. Tasks included passive listening to tones and phonemes while viewing a slideshow of landscape photographs; active listening to phonemes and words to detect targets amid distractors; picture naming; verb generation following auditory presentation of nouns; finger tapping; mouth movement and articulation; simultaneous multimodal (auditory-vibrotactile) stimulus presentation with unimodal target detection; auditory n-back task (phoneme stimuli); visual search task; visual silent reading task; facial emotion recognition task; and motor, auditory, and tactile imagery. Not all patients engaged in all tasks.

ECOG RECORDING AND ELECTRODE LOCALIZATION

The electrode grids used to record ECoG for this study were 64-channel 8x8 arrays of platinum-iridium electrodes. In these arrays, each electrode is a 4 mm diameter disk with 2.3 mm exposed (thus 2.3 mm effective diameter), with 10 mm center-to-center spacing between adjacent electrodes. The recording system used for clinical monitoring does not permit monitoring of the high gamma band (80-150 Hz) due to low-pass filtering constraints. Therefore, the signal for the ECoG grid was split and sent to both the clinical system and a custom recording system. An electrode at the corner of the grid (see Fig. 1A) was used as reference potential for all other grid electrodes. The ECoG for patients 1-4 was amplified x10000 and analog filtered 0.01-250 Hz, while the ECoG for patient 5 was amplified x5000 and analog filtered 0.01-1000 Hz. Signals were digitized at 2003 Hz with 16 bit resolution. ECoG was recorded in separate blocks approximately 3-8 minutes in length, corresponding to the different behavioral tasks performed.

Preoperative structural MR images were acquired on all patients with a 1.5T MRI scanner. CT scans were acquired postoperatively with subdural electrodes in place, clearly showing electrode positions with respect to skull geometry. Initial coregistrations were obtained between postoperative CT and preoperative MRI scans using SPM2 (http://www.fil.ion.ucl.ac.uk/spm/software/spm2). 3-D brain renderings were then generated from the MRI volume using MRIcro (http://www.sph.sc.edu/comd/rorden/mricro.html), and overlaid with the coregistered CT volume for an initial estimate of electrode positions. As

necessary, these coregistrations were manually corrected using electrode positions from intraoperative photographs as well as known electrode coordinates recorded with a StealthStation stereotactic system.

ANALYSIS

All analyses were done using MATLAB. Prior to any further processing, channels with a low signal-to-noise ratio (SNR) were identified and deleted. Reasons for low SNR included 60 Hz line interference, electromagnetic noise from hospital equipment, and poor contact with cortical surface. The raw time series, voltage histograms, and power spectra were used to identify noisy channels. Two investigators had to both agree before a noisy channel was dropped. This resulted in 2 channels dropped for patient 1, 3 channels dropped for patient 2, 12 channels dropped for patient 3, 4 channels dropped for patient 4, and no channels dropped for patient 5. The multi-channel ECoG was digitally re-referenced to a common average and high-pass filtered above 2.3 Hz with a symmetrical (phase true) finite impulse response (FIR) filter (~35 dB/octave roll-off) in order to minimize heartbeat artifact. Single channels of this minimally-processed ECoG are referred to as the 'raw signal' $x_{RAW}(t)$ in the following analyses.

To create Fig. 1B (bottom), 2000 ms epochs centered on the time points identified as theta troughs were extracted from the raw signal and averaged to produce the theta-trough locked event-related potential (ERP). The time series indices corresponding to theta troughs were extracted from the theta (4-8 Hz) band analytic phase time series $\phi_{TH}(t)$.

To create $\phi_{TH}(t)$, first the raw signal $x_{RAW}(t)$ from one recording block (6 minutes 7 seconds, subject 1, electrode number 8, see Fig. 1A) was filtered from 4-8 Hz in order to create the real-valued band-pass filtered signal $x_{TH}(t)$. All filtering was done with a two-way least-squares FIR filter (eegfilt.m from the EEGLAB toolbox, (1)). Second, the complex-valued analytic signal $z_{TH}(t)$ was created by applying the Hilbert Transform H (2), where $z_{TH}(t) = x_{TH}(t) + i$ $H[x_{TH}(t)]$. Third, the phase at each time point was extracted from $z_{TH}(t)$ in order to create the analytic phase time series $\phi_{TH}(t)$. $\phi_{TH}(t)$ assumed values within $(-\pi, \pi]$ radians, where π radians corresponds to a theta trough and 0 radians corresponds to a theta peak (cosine phase). Theta troughs were identified as all local minima of $\phi_{TH}(t)$ less than $(-\pi + 0.01)$. This produced N=2223 locking events.

The ERP voltage at each time point was compared to a parametric reference distribution in order to determine (uncorrected) statistical significance (not shown in Fig. 1). This reference distribution was the best Gaussian fit of a set of voltage values produced by time-locked averaging the raw signal. Twenty five hundred sets of resampled or surrogate indices were used for locking. Each set of surrogate points was created by shifting the 2223 real theta trough indices forward or backward by the same randomly chosen integer lag, modulo the length of the raw time series. This preserves both the number of locking indices and the interval between sequential indices, assuring that the real and surrogate indices both have the same statistical properties. Given that the filtered ECoG is not a perfect sinusoid, these surrogate indices are shifted away from the actual theta troughs and will be more uniformly distributed relative to the phase of the ECoG theta oscillation. The distribution of 2500 voltage values generated by locking and averaging the raw signal to the surrogate indices was then fit with a Gaussian. Note that while the histogram of raw ECoG voltage values is super-Gaussian (leptokurtic), the distribution of ERP voltage values approaches a Gaussian distribution by the Central Limit

Theorem. The actual ERP voltage at each time point was compared to this Gaussian distribution in order to acquire an uncorrected two-tail probability.

To create Fig. 1B (top), a set of normalized instantaneous power time series $\{P_{BP}(t)\}_{NORM}$ was constructed. First, the raw signal $x_{RAW}(t)$ was separated into bands with center frequencies ranging from 10 Hz to 224 Hz, in 2 Hz steps with 4 Hz bandwidths. This created a set of real-valued band-pass filtered signals $\{x_{BP}(t)\}$. Second, each $x_{BP}(t)$ was normalized by subtracting the temporal mean and dividing by the temporal standard deviation in order to create the set of normalized band-passed signals $\{x_{BP}(t)\}_{NORM}$. Normalization was done in order to facilitate comparison between different frequency bands. Third, the Hilbert Transform H was applied to each signal in $\{x_{BP}(t)\}_{NORM}$ to create the set of normalized complex-valued analytic signals $\{z_{BP}(t)\}_{NORM}$. Fourth, the absolute value of each analytic signal was taken to produce the set of normalized analytic amplitude time series $\{A_{BP}(t)\}_{NORM}$. Fifth, each amplitude time series was squared (element-wise) to produce the set of normalized instantaneous power time series $\{P_{BP}(t)\}_{NORM}$. Sixth, 2 second epochs centered on the 2223 time points identified as theta troughs were extracted from $\{P_{BP}(t)\}_{NORM}$ and averaged within each band in order to produce the theta-trough locked trace of mean instantaneous power across frequencies. Seventh, uncorrected p-values for each time point in each band were determined as above for the ERP. Eighth, a false discovery rate (FDR) correction with $\alpha = 0.001$ was applied to the uncorrected p-values for each time point in each band (including the ERP) in order to correct for multiple comparisons (3).

To create Fig. 1C, high gamma amplitudes were extracted and binned as a function of theta phase. First, $x_{RAW}(t)$ for the same electrode as in Fig. 1B was extracted for each recording block of ECoG data. $x_{RAW}(t)$ was band-pass filtered from 80 to 150 Hz, the Hilbert Transform applied, the absolute value taken, and the results for all blocks concatenated in order to create the high gamma analytic amplitude time series $A_{HG}(t)$. Next, theta troughs were identified as above, with theta peaks defined as all local minima of $(\phi_{TH}(t) + \pi)$ which were less than $(-\pi + 0.1)$. Finally, the values of $A_{HG}(t)$ occurring at points corresponding to a theta peak or trough were binned into 1 of 2 sets and each set fit with a gamma distribution (4). The confidence intervals generated during parameter estimation were used to determine significance ($p<0.001$).

Fig.s 1D, 2, 3, and S4-8 make use of the modulation index M. This index takes advantage of the complex-valued signals produced by most frequency and time-frequency transforms. For example, define the real-valued signal $x_{HG}(t)$ to be the ECoG from one channel after band-pass filtering from 80 to 150 Hz (Fig. S1A). Applying the Hilbert Transform $y_{HG} = H(x_{HG})$ converts this real-valued signal into an analytic, complex-valued signal of the form $z_{HG}(t) = x_{HG}(t) + i\ y_{HG}(t) = A_{HG}(t)\ e^{i\phi_{HG}(t)}$, where $A_{HG}(t)$ is the high gamma analytic amplitude time series (also called the amplitude envelope) and $\phi_{HG}(t)$ is the high gamma analytic phase time series. Similarly, we can construct the analytic signal for the theta band: $z_{TH}(t) = x_{TH}(t) + i\ y_{TH}(t) = A_{TH}(t)\ e^{i\phi_{TH}(t)}$ (Fig.s S1B-E).

To determine the modulation index M, we first construct a composite complex-valued signal by combining the amplitude time series of one frequency with the phase time series of the other. There are two such possible composite signals including the one of interest here, which combines the HG amplitude with the theta phase: $z(t) = A_{HG}(t)\ e^{i\phi_{TH}(t)}$ (Fig. S1F). At each sample point this composite signal takes on some particular value in the complex plane (Fig.s S2A-D). If the probability density function (PDF) of z (Fig. S2E) is not radially symmetric, then it must be the case that either 1) A_{HG} and ϕ_{TH} share mutual information, or 2) the distribution of ϕ_{TH} is nonuniform. Measuring the degree of asymmetry of this PDF, as can be done by computing the

3

mean or first moment M of z(t), provides a useful metric of coupling between the two time series.

Since the question of interest is the degree of coupling between A_{HG} and ϕ_{TH}, rather than the statistical properties of either A_{HG} and ϕ_{TH} examined alone, the mean M must first be normalized before it can be used as a metric of coupling strength. That is, we are interested in the properties of the joint distribution of A_{HG} and ϕ_{TH} taking into account the particular forms of the marginal distributions of A_{HG} alone and ϕ_{TH} alone. One way to accomplish this is to compare the actual mean M (call it M_{RAW}) to a set of surrogate means $\{M_{sur}\}$ created by offsetting A_{HG} and ϕ_{TH} by some large time lag. That is, we introduce a time lag τ between A_{HG} and ϕ_{TH} such that the composite signal is a function of both time and lag: $z(t, \tau) = A_{HG}(t + \tau) \, e^{i\phi_{TH}^{(t)}}$. Note that the dependence (if any) between A_{HG} and ϕ_{TH} will be a function of the lag τ between them, decreasing for large τ, while τ has no effect on the distribution of ϕ_{TH} alone or A_{HG} alone. Therefore, any asymmetry in the distribution of $z(t, \tau)$ at large τ will be due to the nonuniformity of ϕ_{TH}, while the scale (how far points fall from the origin) will be determined by A_{HG} alone. The modulus or length of M_{RAW}, compared to the distribution of surrogate lengths, provides a measure of the coupling strength, while the angle of M, compared to the distribution of surrogate angles, indicates the phase of theta associated with the largest HG amplitudes (Fig. S3). We can define a normalized or z-scored length $M_{NORM} = (M_{RAW}-\mu)/\sigma$, where μ is the mean of the surrogate lengths and σ their standard deviation. This normalization insures that M_{NORM} is insensitive to the marginal distributions of A_{HG} and ϕ_{TH} and is sensitive only to their joint distribution, as desired. In particular, for a given number of sample points within a recording block, we can directly compare this metric for cross-frequency coupling strength across different channels as well as different frequency bands which may have very different power levels. Also, since all recording blocks used were of similar duration, comparisons across different blocks is valid. Furthermore, this metric corresponds to a zscore and can be used to determine the probability that such a result would have been due to chance. Therefore, we define this normalized metric $M_{NORM}(\tau)$ as the modulation index used in this paper. With x(t) as the raw signal, in MATLAB code this is:

```
srate=2003;                  %% sampling rate used in this study, in Hz
numpoints=length(x);         %% number of sample points in raw signal
numsurrogate=200;            %% number of surrogate values to compare to actual value
minskip=srate;               %% time lag must be at least this big
maxskip=numpoints-srate;     %% time lag must be smaller than this
skip=ceil(numpoints.*rand(numsurrogate*2,1));
skip(find(skip>maxskip))=[];
skip(find(skip<minskip))=[];
skip=skip(1:numsurrogate,1);
surrogate_m=zeros(numsurrogate,1);
%% HG analytic amplitude time series, uses eegfilt.m from EEGLAB toolbox
%% (http://www.sccn.ucsd.edu/eeglab/)
amplitude=abs(hilbert(eegfilt(x,srate,80,150)));
%% theta analytic phase time series, uses EEGLAB toolbox
phase=angle(hilbert(eegfilt(x,srate,4,8)));
%% complex-valued composite signal
z=amplitude.*exp(i*phase);
%% mean of z over time, prenormalized value
m_raw=mean(z);
%% compute surrogate values
    for s=1:numsurrogate
        surrogate_amplitude=[amplitude(skip(s):end) amplitude(1:skip(s)-1)];
        surrogate_m(s)=abs(mean(surrogate_amplitude.*exp(i*phase)));
        disp(numsurrogate-s)
    end
%% fit gaussian to surrogate data, uses normfit.m from MATLAB Statistics toolbox
[surrogate_mean,surrogate_std]=normfit(surrogate_m);
%% normalize length using surrogate data (z-score)
m_norm_length=(abs(m_raw)-surrogate_mean)/surrogate_std;
m_norm_phase=angle(m_raw);
m_norm=m_norm_length*exp(i*m_norm_phase);
```

Note that this method can also be applied to band-passed signals from two different electrodes in order to measure cross-frequency, cross-electrode coupling. One reason we chose to use this index rather than a different index such as linear or phase coherence between the HG amplitude envelope and the theta band-passed signal because it is more sensitive to certain types of nonlinear coupling between amplitude and phase time series. As one example, consider a HG amplitude envelope which has a constant mean value (say, 2 microvolts) with small gaussian random noise (say, mean of 0 microvolts and standard deviation of 0.1 microvolts). Stipulate that this envelope has a transient increase of short duration (say, 30 ms). This transient increase occurs at every theta trough with a probability of 0.5, at every theta peak with a probability of 0.5, and with a probability of 0 at every other phase. Further stipulate that the maximum amplitude reached at these two theta phases is different (say, 4 microvolts maximum amplitude if the transient occurs at the theta peak, but 10 microvolts if the transient occurs at the theta trough). This synthetic signal can be viewed as a very simple model of the activation and refractory period of a local neuronal population in a given cortical area. In this simple case, both linear and phase coherence between the HG amplitude envelope and the theta filtered signal will be at chance levels despite the fact that the amplitude time series is a direct function of theta phase, while the normalized modulation index used here will detect very strong and significant coupling, as it should. Coherence is a linear measure which does not perform well given the nonlinear and stochastic nature of this strong coupling, making the modulation index used here a more appropriate tool to use in the analysis of theta/HG coupling.

To create Fig. 1D, first the raw signal $x_{RAW}(t)$ from 1B was separated into bands with center frequencies from 5 Hz to 200 Hz, in 5 Hz steps with 4 Hz bandwidths. This created a set of 40 real-valued band-pass filtered signals $\{x_{AMPLITUDE\_BP}(t)\}$. Second, a different set of 19 real-valued band-pass filtered signals $\{x_{PHASE\_BP}(t)\}$ was created by filtering the raw signal $x_{RAW}(t)$ with center frequencies from 2 Hz to 20 Hz, in 1 Hz steps with 1 Hz bandwidths. Third, the Hilbert Transform was applied to both sets to generate complex-valued analytic band-passed signals. Fourth, the absolute value of $\{x_{AMPLITUDE\_BP}(t)\}$ taken to create a set of analytic amplitude time series $\{A_{BP}(t)\}$ and the phase of $\{x_{PHASE\_BP}(t)\}$ was extracted to create a set of analytic phase time series $\{\phi_{BP}(t)\}$. Fifth, the normalized modulation index described above was computed for all pairs of amplitude and phase time series, generating 760 index values. Sixth, a statistical significance threshold was established after Bonferroni correction for multiple comparisons. With $\alpha = 0.001$ and $N = 760$ comparisons, an index value greater than 4.7 was required for significance.

A similar procedure was used to create Fig. S4. First, the raw signal $x_{RAW}(t)$ from all electrodes in one recording block in all subjects was bandpassed in the HG range and the analytic amplitudes extracted. Second, a set of 28 real-valued band-pass filtered signals $\{x_{PHASE\_BP}(t)\}$ was created by filtering the raw signal $x_{RAW}(t)$ with center frequencies from 3 Hz to 30 Hz, in 1 Hz steps with 1 Hz bandwidths. Third, the modulation index between the HG analytic amplitudes and all phase time series was computed. Fourth, the mean modulation index value across all electrodes and subjects was computed, with standard error estimated with bootstrap resampling.

To create Fig.s 2 and S6-7, the zero-lag modulation index value between HG amplitude and theta phase was computed as described above for each electrode in each subject for each task, resulting in 4081 values. In addition, the mean HG and theta amplitudes were computed for all electrodes in all subjects for each task. With $\alpha = 0.01$ and $N = 4081$ comparisons, an index value greater than 4.57 was required for significance (red line in Fig. 2A). Only points with modulation index values greater than 4.57 were used for computing the correlations for Fig.s 2B-

C. Intermediate variables generated while computing the normalized modulation index were used to create Fig.s S6-7.

To create Fig.s 3A and S8, first all recording blocks for each subject were concatenated and filtered in the HG and theta bands. Second, the modulation index $M(\tau)$ was computed for all electrodes at a series of lags from -1000 ms to 1000 ms in 25 ms steps. Third, a recursive procedure was used to determine the lag τ_{max} producing the largest $|M(\tau)|$ for each electrode at a temporal resolution of 0.5 ms (the limit set by the sampling rate). In this case, 1000 surrogate values were used rather than 200 as for the block-specific analyses. Fourth, the modulation index value at τ_{max} was used to get an uncorrected, two-tailed p-value. Fifth, two FDR corrections were applied after acquiring uncorrected p-values for all electrodes in all subjects. The first FDR correction, with $\alpha = 0.05$, was used to determine which channels to include in Fig.s 3A and S8 (292 out of 299 tested channels, 97.7%). The second FDR correction, with $\alpha = 0.001$, was reported in the main text (254 out of 299 tested channels, 84.3%). For subject-specific information, see CLINICAL INFORMATION AND ADDITION TESTS.

To create Fig.s 3B-E, first the block-specific modulation index values were computed for all electrodes and tasks in all subjects. Second, the difference between the length of the block-specific modulation index from the mean modulation index value for all tasks recorded that day was computed for each subject. This list of block-specific differences for all electrodes in one subject was termed the spatial pattern vector for that task. Fig.s 3B-C display this spatial pattern for two different tasks in subject 5. Third, for each subject, each pair of recording blocks was labeled SIMILAR or DIFFERENT depending on which task the patient was performing for each block. For example, a pair of recording blocks acquired during a verb generation task would be labeled SIMILAR, while a verb generation block and a visual picture naming block would be labeled DIFFERENT. Fourth, the correlation coefficient between the spatial pattern vectors for each block in subject 5 was computed and is shown in Fig. 3D with tasks grouped according to similarity. For Fig. 3D, the task list is: 1-4, passive auditory listening to tones or phonemes; 5, mouth motor activation; 6, verb generation; 7, hand motor activation; 8-11 auditory working memory; 12-13, linguistic target detection; 14-17, auditory-vibrotactile target detection. Note that tasks are not ordered chronologically, and that while similar tasks are grouped together, the specific ordering of tasks within a group as well as the ordering between separate groups is arbitrary. To create Fig. 3E, the mean correlation between spatial pattern vectors for the 58 task pairs in the SIMILAR category was computed, and as was the mean correlation between spatial pattern vectors for the 617 task pairs in the DIFFERENT category. Bootstrap resampling was used to determine the standard error of this estimate of the mean.

To create Fig. S5A, first HG analytic amplitude time series were generated for 2 electrodes from a recording block where the subject passively heard a series of tones while watching a slideshow. Second, 480 epochs (600 ms) centered on the tone onset were extracted from the HG time series. Third, the mean HG amplitude trace (over epochs) was computed. Fourth, traces were baseline corrected by subtracting the mean HG amplitude for all prestimulus sample points over all epochs from each trace. Fifth, bootstrap resampling was used to estimate the standard error for each time point. An event-related change in HG amplitude was considered significant if it remained at least 3 standard deviations away from the baseline-corrected prestimulus mean of zero for at least 50 ms using the surrogate procedure used to determine significance for Fig. 1B. Sixth, zero-lag modulation index values for HG amplitude and theta phase were computed for these electrodes as above.

To create Fig. S5B, first HG analytic amplitude time series and theta analytic phase time series were generated for all electrodes in all subjects from a recording block where the subjects were engaged in an auditory linguistic target-detection task. Second, sample points no more than 500 ms before a stimulus onset were labeled PRESTIMULUS, while sample points no more than 500 ms after stimulus onset were labeled POSTSTIMULUS. Points not within these ranges were discarded. Third, modulation index values were computed for the PRESTIMULUS and POSTSTIMULUS sets separately. Fourth, the mean modulation index value over all electrodes in all subjects was computed. Bootstrap resampling was used to estimate the standard error. Since the difference in the mean modulation index value for the PRESTIMULUS and POSTSTIMULUS sets is much less than the standard error, the mean modulation index values are not significantly different.

To create Fig. S2E, the high gamma amplitude was sorted by theta phase and a fit with a parametric distribution. First, each value of $\phi_{TH}(t)$ was rank-ordered from $(-\pi,\pi]$ and placed into one of 32 equal sized bins. The mean phase in each bin was identified as the bin phase $\phi_1, \phi_2, \ldots,$ ϕ_{32}. Second, for each time point t, $A_{HG}(t)$ was assigned a bin phase from $\phi_1, \phi_2, \ldots, \phi_{32}$ and sorted into one of 32 bins $A_1, A_2, \ldots, A_{32}$ as a function of the phase value $\phi_{TH}(t)$ occurring at that time. Fourth, a gamma distribution was fit to each amplitude set $A_1, A_2, \ldots, A_{32}$, producing 2 parameters for each bin phase (gamfit.m, part of the Statistic toolbox in MATLAB). Fifth, for each bin phase at 100 equally spaced points representing amplitude from 0 to 5 μV, a gamma probability density function was generated. That is, the probability density p was estimated for the 3200 points corresponding to 100 values of high gamma amplitude occurring at each of 32 different theta phases. Sixth, intermediate values were linearly interpolated before plotting (griddata.m).

CLINICAL INFORMATION AND ADDITIONAL TESTS
(supporting online text)

CLINICAL INFORMATION

Subject 1 was a 37 year old right handed woman with medically intractable complex partial seizures. MRI was normal, PET scan showed left temporal hypometabolism. She had a left anterior temporal lobectomy including the left amygdala and anterior hippocampus. Pathology showed left mesial temporal sclerosis. Considering all tested electrodes, 62/62 (100%) channels showed significant theta/high gamma coupling at $p < 0.001$ after false discovery rate (FDR) correction for multiple comparisons. Considering electrodes over resected tissue only, 9/9 (100%) channels were significant at $p < 0.001$. Considering only electrodes not over resected tissue, 53/53 (100%) channels were significant at $p < 0.001$. Please note that "resected tissue" does not imply only epileptic tissue. The neurosurgeon often removes a variable amount of histologically and electrophysiologically normal tissue surrounding an epileptic focus.

Subject 2 was a 45 year old right handed woman with intractable complex partial seizures. MRI showed abnormal signal and thinning of the left frontal opercular cortex and insular cortex, as well as diminished size of the left hippocampus. She had resection of a portion of the left frontal lobe and left amygdala and hippocampus. Pathology showed cortical dysplasia. Considering all tested electrodes, 48/61 (78.7%) channels showed significant theta/high gamma coupling at $p < 0.001$ after false discovery rate (FDR) correction for multiple comparisons. Considering electrodes over resected tissue only, 8/11 (72.7%) channels were significant at $p < 0.001$. Considering only electrodes not over resected tissue, 40/50 (80%) channels were significant at $p < 0.001$.

Subject 3 was a 35 year old right handed woman with a left temporal abscess in childhood resulting in intractable complex partial seizures. MRI showed a small resection cavity in the anterior inferior left temporal lobe, a small area of gliosis in the left cingulate gyrus, and subtle changes in the left hippocampal body and tail. She had a left anterior temporal lobectomy including amygdala and anterior hippocampus. Pathology showed gliosis and hippocampal sclerosis. Considering all tested electrodes, 41/52 (78.8%) channels showed significant theta/high gamma coupling at $p < 0.001$ after false discovery rate (FDR) correction for multiple comparisons. Considering electrodes over resected tissue only, 10/12 (83.3%) channels were significant at $p < 0.001$. Considering only electrodes not over resected tissue, 31/40 (77.5%) channels were significant at $p < 0.001$.

Subject 4 was a 24 year old left handed woman who had childhood meningitis and cerebritis with a stroke, and intractable complex partial seizures. MRI showed encephalomalacia in the left partietal lobe. She had a left anterior temporal lobectomy including amydala and anterior hippocampus. Pathology was reported as gliosis. Considering all tested electrodes, 38/60 (63.3%) channels showed significant theta/high gamma coupling at $p < 0.001$ after false discovery rate (FDR) correction for multiple comparisons. Considering electrodes over the encephalomalacia left by the childhood stroke and the electrodes over resected tissue, 5/20 (25%) channels were significant at $p < 0.001$. Considering only the remaining electrodes not over the gap or resected tissue, 33/40 (82.5%) channels were significant at $p < 0.001$.

Subject 5 was a 37 year old right handed woman with reflex epilepsy: reading-induced seizures consisting of word blindness, and then a subjective feeling that she was losing awareness of her surroundings. MRI showed left mesial temporal sclerosis. She had a left posterior inferior temporal resection. Pathology was reported as gliosis and focal neuronal loss. Considering all tested electrodes, 63/64 (98.4%) channels showed significant theta/high gamma coupling at $p < 0.001$ after false discovery rate (FDR) correction for multiple comparisons. Considering electrodes over resected tissue only, 8/8 (100%) channels were significant at $p < 0.001$. Considering only electrodes not over resected tissue, 55/56 (98.2%) channels were significant at $p < 0.001$.

ADDITIONAL TESTS

Here we address 4 potential confounds to our data. The first consideration is that the theta/HG coupling reported here is an artifact of flawed signal processing or analysis. One possibility is that theta/HG coupling is an artifact of a particular time-frequency decomposition and would disappear if another were used. Multiple different time-frequency decompositions (short-time Fourier transform, wavelet transform, band-passed locked averaging, Hilbert transform, Hilbert-Huang transform, etc.) were used in the analysis of a subset of channels of one subject before all channels in all subjects were examined. Each of these decompositions showed evidence of significant coupling, indicating that the coupling observed is not dependent upon any particular time-frequency analysis algorithm or settings.

A second issue to consider stems from the power-law distribution of power as a function of frequency in the ECoG signal. This means that the low frequency components of the ECoG are much larger in amplitude than the high frequency components. As an example, the theta-filtered waveform is typically 10-20 times larger in amplitude than the HG-filtered waveform. Perhaps the filtering process is incomplete and residual features of the theta waveform remain in the HG filtered signal and distort further analyses. This would be unusual, given the known filter properties. However, several different empirical tests of this possibility (not shown) using synthetic data and mixed synthetic-empirical data make this unlikely.

In one such mixed test, an ECoG channel is first filtered in the theta and HG ranges and then one or both time series are scaled by different fixed constants. These two signals are added back together and the sum treated as a raw signal and taken through the entire analysis procedure. If neither time series is rescaled, there is no change in the significance of coupling, as expected. If the theta filtered time series alone is rescaled (which has no effect on theta phase), there is no effect on the HG signal or the final modulation index, demonstrating that coupling is not the result of theta power 'seeping through' the band-pass filter. If the HG time series alone is rescaled, the length of the prenormalized modulation index does change (as it is sensitive to high gamma amplitude), but the normalized modulation index does not (since the surrogate distribution is rescaled by the same factor). If the ratio of power in the two bands was an important factor in the analysis which could lead to artifacts, then one would expect significantly different coupling strengths to result. In fact, no such differences were found in several tests of randomly selected channels, supporting the claim that the modulation of theta/HG coupling strength by theta power is the result of interacting neuronal populations rather than analysis artifacts.

A third potential confound is that the analysis procedure shows a systematic bias and therefore coupling would be found whether or not it was actually present in the signal. Again, several different empirical tests of this possibility (not shown) using synthetic data and mixed synthetic-actual data make this unlikely. In one such test, theta and HG filtered signals are extracted, the HG filtered signal shifted by a fixed time lag before the two time series were added together and then run through the entire analysis procedure. Here the statistics of the HG and theta filtered time series are preserved but the amplitude-phase relationship between them is not. In this case no coupling was found. In a second test, the HG analytic amplitude time series $A_{HG}(t)$ was replaced with a surrogate amplitude time series $A_S(t) = [1+a_1+a_2\cos(\pi+\phi_{TH}(t))] A_{HG}(t)$ for several different values of the parameters a_1 and a_2 from 0 to 1. If $a_2 = 0$ and $a_1 = 1$, then $A_S(t) = 2 A_{HG}(t)$ and the length of the prenormalized modulation index $|M_{RAW}|$ will be twice as long. One can ask which value of a_2 is required when $a_1 = 0$ in order to double the prenormalized $|M_{RAW}|$. The ratio of a_1 to a_2 provides a measure of the relative sensitivity of the analysis procedure to non-specific versus theta phase-specific changes in HG amplitude. For actual data from several channels, a mean value of $a_2 = 0.083$ is required, meaning that the length of the prenormalized modulation index is 12 times more sensitive to phase-specific changes in amplitude. Furthermore, since nonspecific changes in amplitude will scale the surrogate distribution by the same degree, changes in a_1 (but not a_2) are invisible to the normalized modulation index used here. By letting a_2 assume negative values, we can thus 'extract' the theta phase modulation of HG amplitude such that $|M|$ for the surrogate amplitude time series approaches zero. This shows that the analysis procedure used is extremely sensitive to phase modulation of amplitude and that the statistical tests are immune to global rescaling of amplitudes.

Computing the modulation index as a function of lag provides another avenue of addressing the above issues. The fact that coupling strength drops as a function of lag argues against a systematic bias for detecting spurious coupling. The coupling strength at large lags is used to create a surrogate distribution against which the significance of coupling at small lags is tested. Therefore, a systematic bias would force coupling at small lags to not be significant.

A fourth potential confound is that the observed coupling may be an artifact of event-related changes in the ECoG caused by stimulus onsets or motor responses. Fig. S4A shows an example of the event-related changes in HG amplitude in response to auditory presentation of tones. The electrode which shows strong event-related HG amplitude modulation does not show significant theta/HG coupling, while the electrode which does not show event-related amplitude modulation shows strong theta/HG coupling. This is in accord with our informal observations that the strongest coupling in all subjects tends to occur at electrodes which show weak event-related responses, with the strongest coupling tending to occur in frontal and anterior temporal electrodes, consistent with the proposed role of theta/HG coupling in top-down control. More formally, Fig. S4B shows that there is no difference in the mean theta/HG coupling strength pre- to post-stimulus, strong evidence that the observed coupling is not an artifact due to event-related ECoG changes.
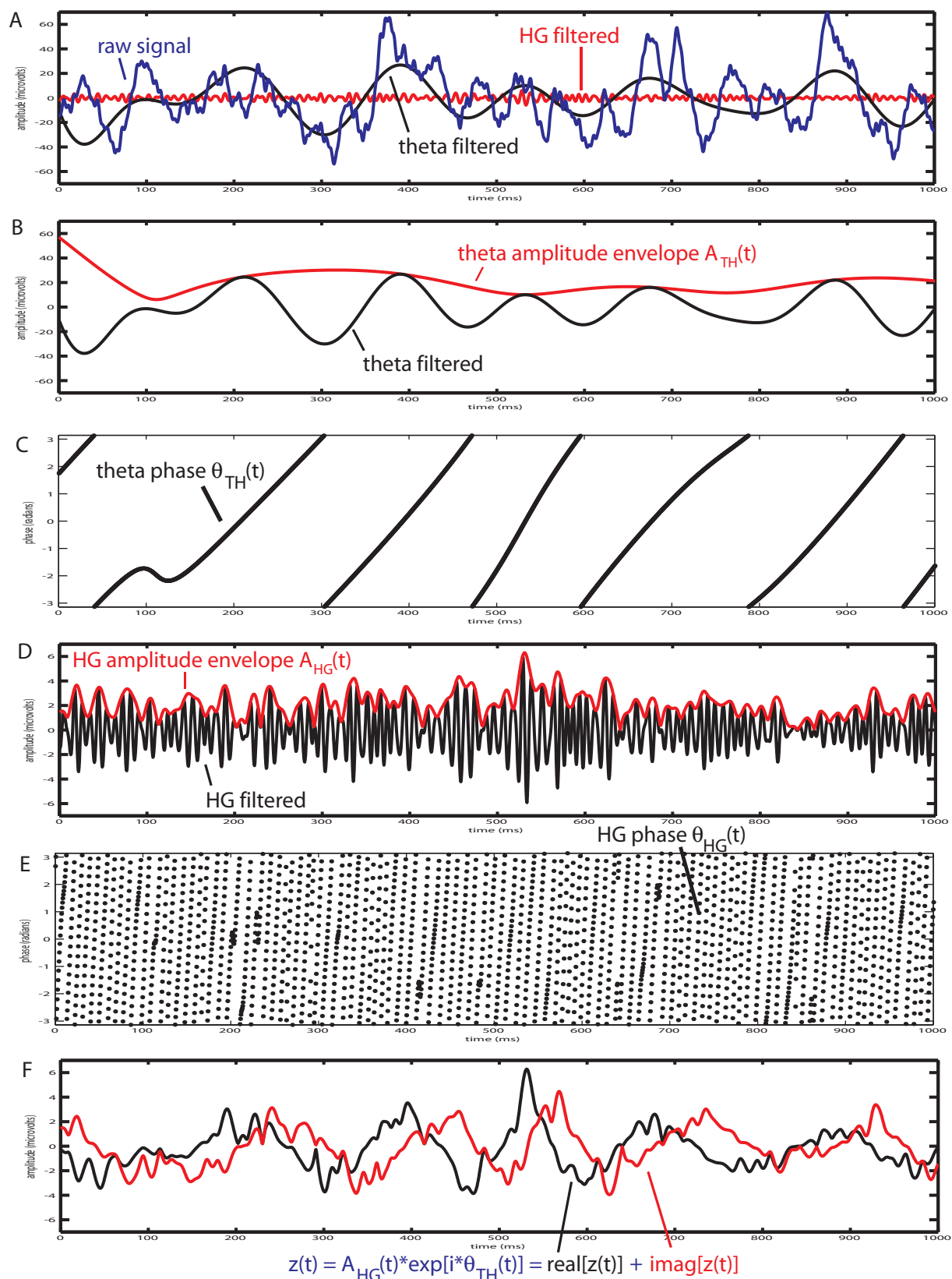
Fig. S1

FIGURE S1. MODULATION INDEX EXAMPLE. A) One second of ECoG data from the same electrode examined in Fig. 1 showing the ECoG signal unfiltered (blue), filtered in the theta (4-8 Hz) range (black), and filtered in the high gamma (80-150 Hz, HG) range (red). B) Theta filtered ECoG from A (black) and the theta analytic amplitude time series (red), which is also known as the amplitude envelope. C) The theta analytic phase time series. D) HG filtered ECoG from A (black) and the HG analytic amplitude time series (red). E) HG analytic phase time series. F) The real (black) and imaginary (red) parts of the complex-valued composite analytic signal z(t) formed by combining the HG analytic amplitude time series with the theta analytic phase time series.
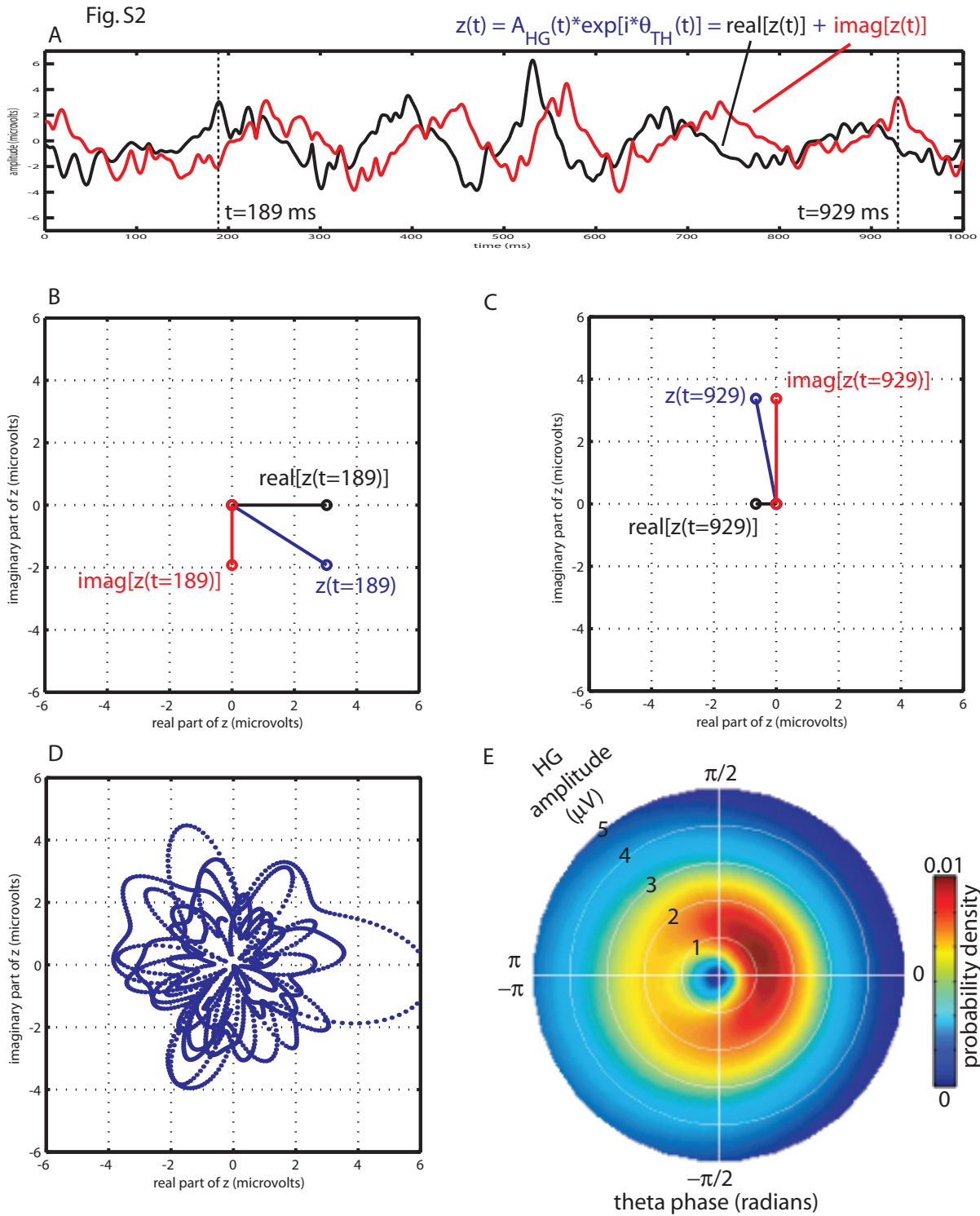
Fig. S2

$$z(t) = A_{HG}(t)*exp[i*\theta_{TH}(t)] = real[z(t)] + imag[z(t)]$$

FIGURE S2. MODULATION INDEX EXAMPLE. A) The real (black) and imaginary (red) parts of z(t) as in Fig. S1F with two time points marked at t = 189 ms and t = 929 ms. B) The value of the composite signal z(t) at t = 189 ms in the complex plane (blue), together with the values of the real (black) and imaginary (red) parts. C) As in B, for t = 929 ms. D) The values of z(t) for all sample points over the one second interval examined. E) The estimated joint probability density function (PDF) for z(t), which can be thought of as a normalized histogram of values assumed by z in the complex plane. Note that if the distribution of theta phase is uniform and the HG amplitude time series and the theta phase time series are statistically independent, then this PDF will be radially symmetric. Since the phase distribution is uniform (data not shown), then any the observed asymmetry must be due to statistical dependence between the two time series.
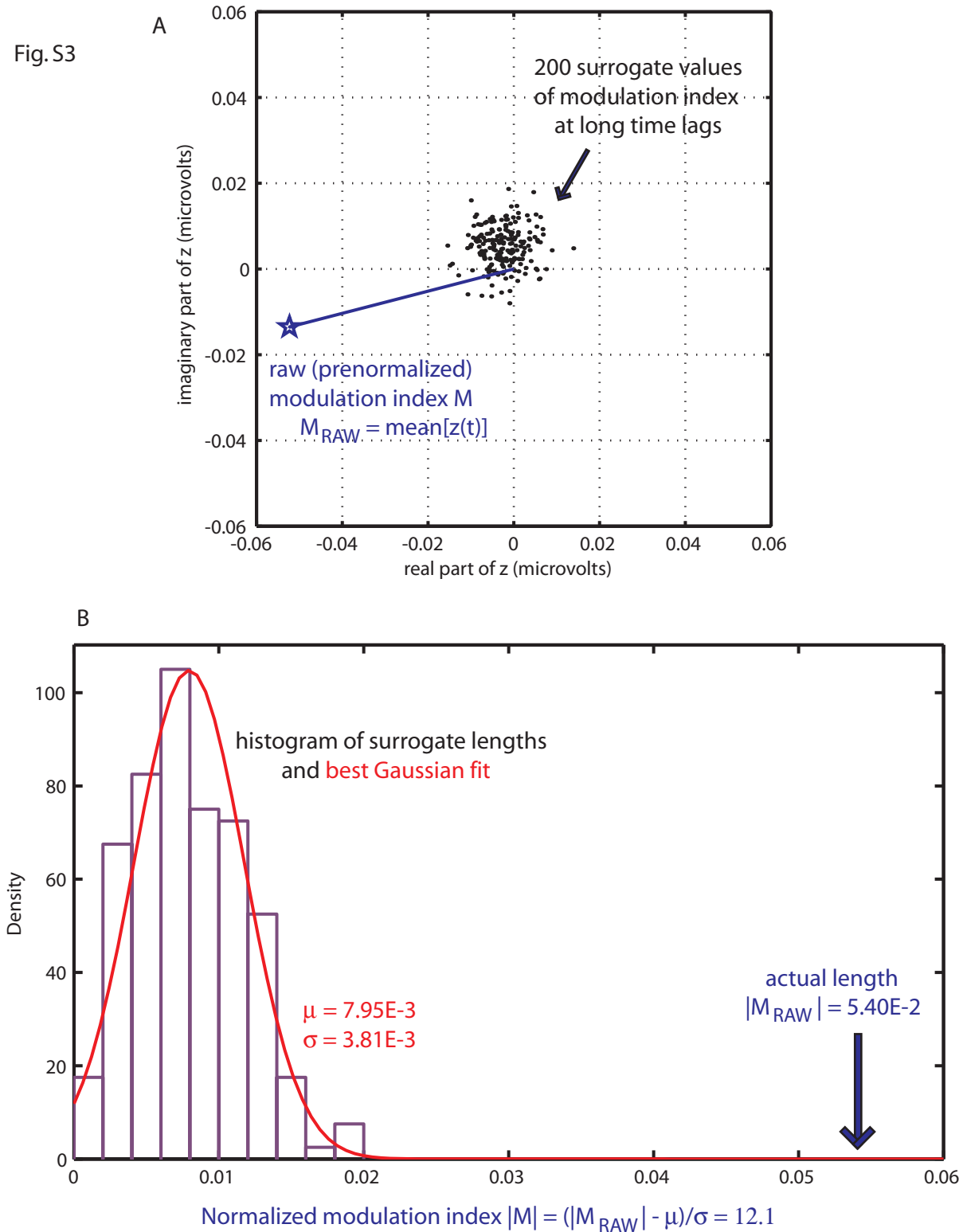
Fig. S3

A

200 surrogate values
of modulation index
at long time lags

raw (prenormalized)
modulation index M
$M_{RAW} = \text{mean}[z(t)]$

B

histogram of surrogate lengths
and best Gaussian fit

$\mu = 7.95E\text{-}3$
$\sigma = 3.81E\text{-}3$

actual length
$|M_{RAW}| = 5.40E\text{-}2$

Normalized modulation index $|M| = (|M_{RAW}| - \mu)/\sigma = 12.1$

FIGURE S3. MODULATION INDEX EXAMPLE. A) The raw modulation index value in the complex plane (blue), which is the temporal mean of z(t), or the first moment of the PDF shown in Fig. S2E. Also shown are 200 surrogate values aquired by computing the modulation index after first shifting the HG amplitude time series and the theta phase time series by some large lag. In this way the statistics of the individual time series are maintained, and only the pairing of sample points between the two time series is changed. Each actual and surrogate modulation index value has a modulus or length (which is used to determine the strength of coupling) and a phase, which indicates where in the low freuqency waveform large analytic amplitudes of the high frequency band tend to occur. All relevant independent statistical biases of the two time series will be reflected by the modulus and phase of the surrogate values. B) The histogram of surrogate lengths (black) and the best fit Gaussian (red). Normalizing the raw modulation index values by the surrogate fits isolates the effect of interest, the statistical dependence between the two time series.

Fig. S4   mean modulation index for high gamma (80-150 Hz)
analytic amplitude and all analytic phases from 3-30 Hz
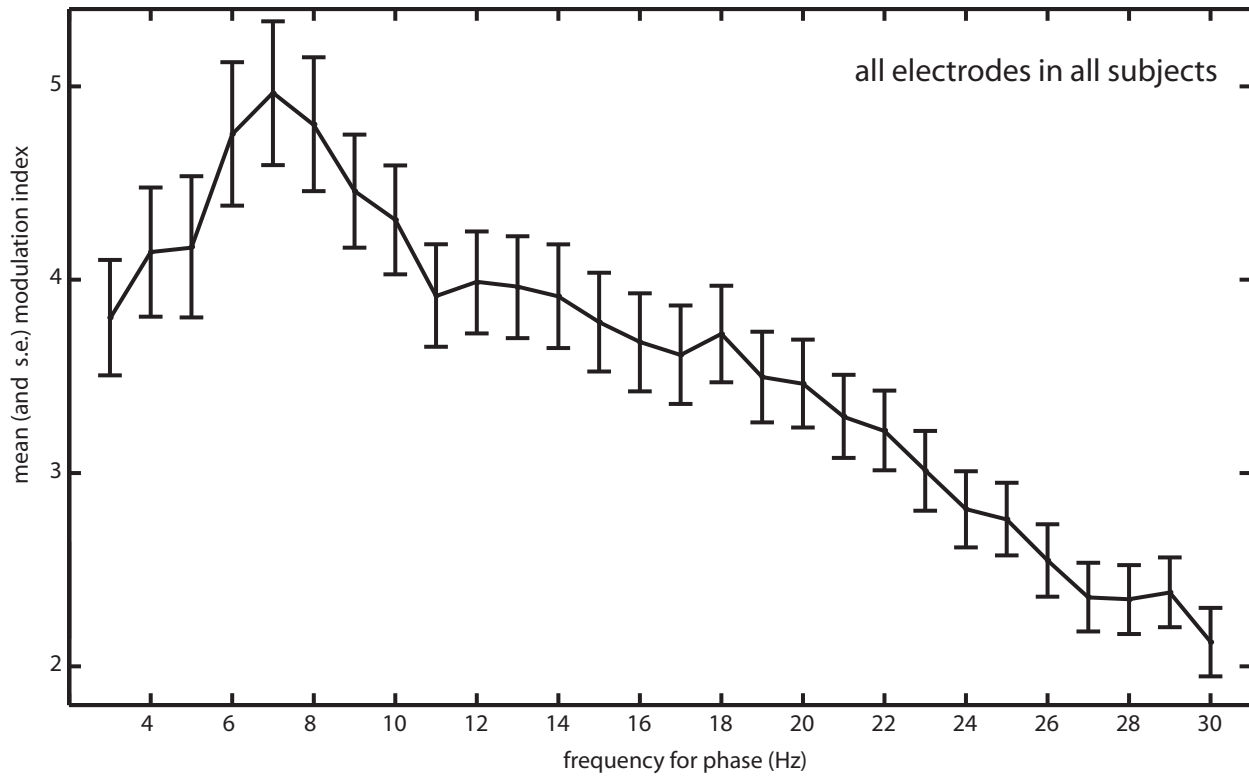
all electrodes in all subjects

FIGURE S4. HG COUPLING IS STRONGEST IN THE THETA BAND. A) The mean strength of coupling across all electrodes in all subjects between the HG amplitude time series and the phase time series for all frequency bands from 3 to 30 Hz. Note that the strongest coupling occurs in the theta band (see also Fig. 1D).
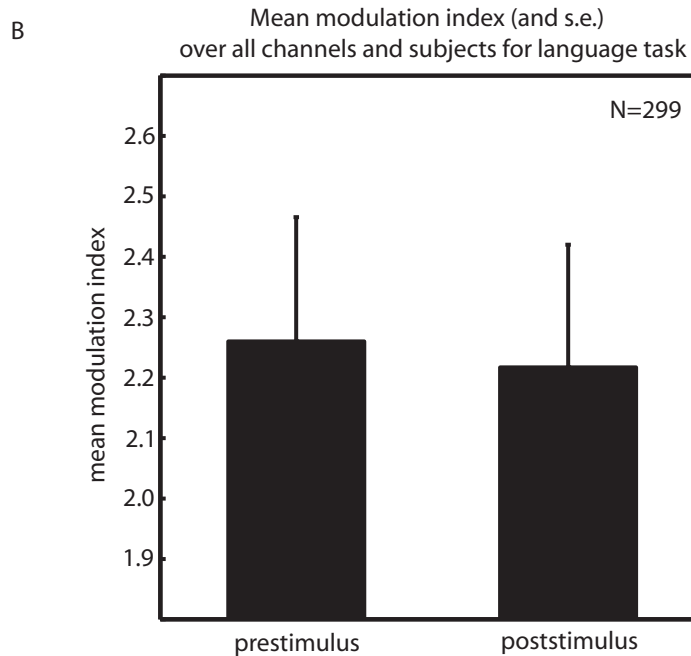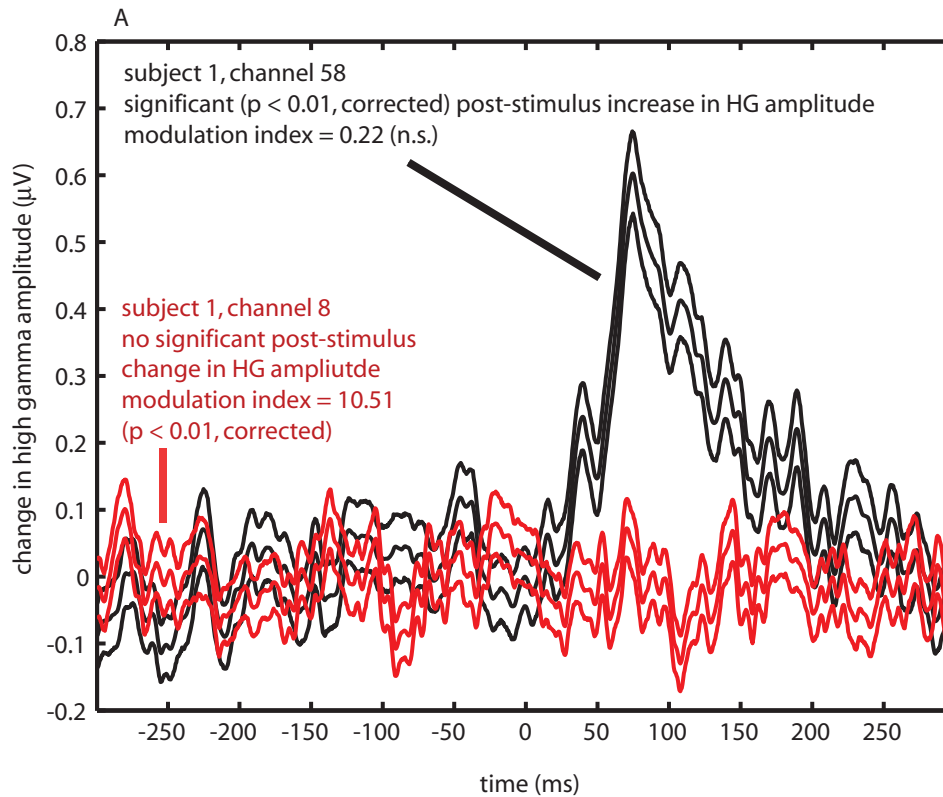
Fig. S5

A

B

FIGURE S5. THETA/HG COUPLING IS NOT ARTIFACT OF EVENT-RELATED CHANGES IN THE ECOG SIGNAL. A) Example of a channel with strong event-related changes in HG amplitude but non-significant theta/HG coupling (black, #58, see Fig. 1A) and a channel with non-significant event-related responses but strong theta/HG coupling (red, #8). Show is the mean change in HG amplitude across epochs (+/- 1 standard error) in response to passively hearing a 100 ms tone while viewing a photographic slideshow. This is in accord with the anecdotal observation that the strongest theta/HG coupling was observed at electrodes which had weak event-related responses, predominantly frontal electrodes. B) The mean modulation index across all electrodes in all subjects computed using only sample points within 500 ms before stimulus onset (prestimulus) or within 500 ms after stimulus onset (poststimulus). If the observed theta/HG coupling were due to event-related changes, the poststimulus modulation index should be significantly different from the prestimulus modulation index, which is not the case.

Fig. S6

A r=0.75631;p=0;N=4081

B r=0.73116;p=0;N=4081

C r=0.27439;p=2.1092e-071;N=4081

D r=-0.13372;p=9.611e-018;N=4081

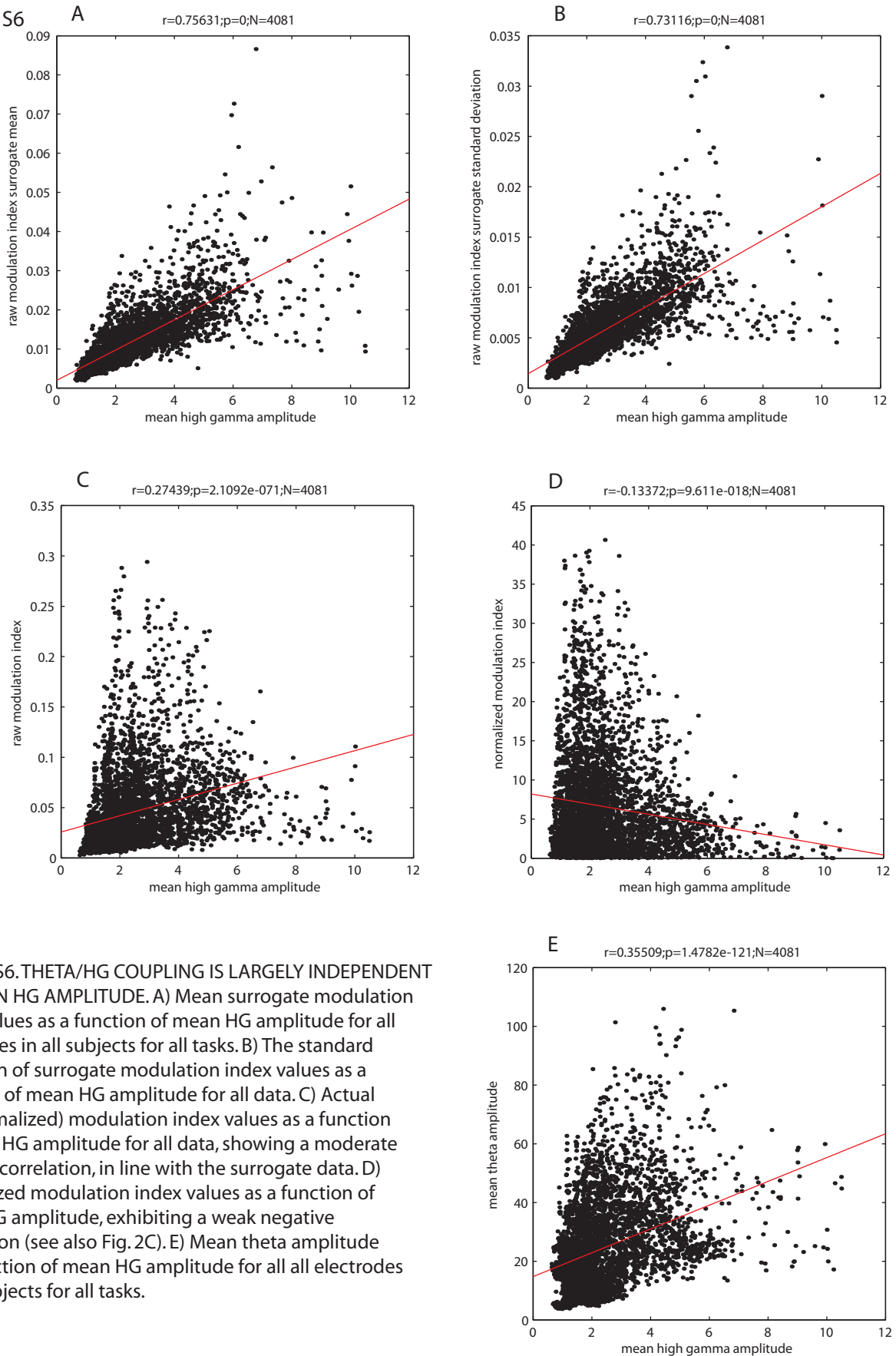**E** r=0.35509;p=1.4782e-121;N=4081

FIGURE S6. THETA/HG COUPLING IS LARGELY INDEPENDENT OF MEAN HG AMPLITUDE. A) Mean surrogate modulation index values as a function of mean HG amplitude for all electrodes in all subjects for all tasks. B) The standard deviation of surrogate modulation index values as a function of mean HG amplitude for all data. C) Actual (prenormalized) modulation index values as a function of mean HG amplitude for all data, showing a moderate positive correlation, in line with the surrogate data. D) Normalized modulation index values as a function of mean HG amplitude, exhibiting a weak negative correlation (see also Fig. 2C). E) Mean theta amplitude as a function of mean HG amplitude for all all electrodes in all subjects for all tasks.
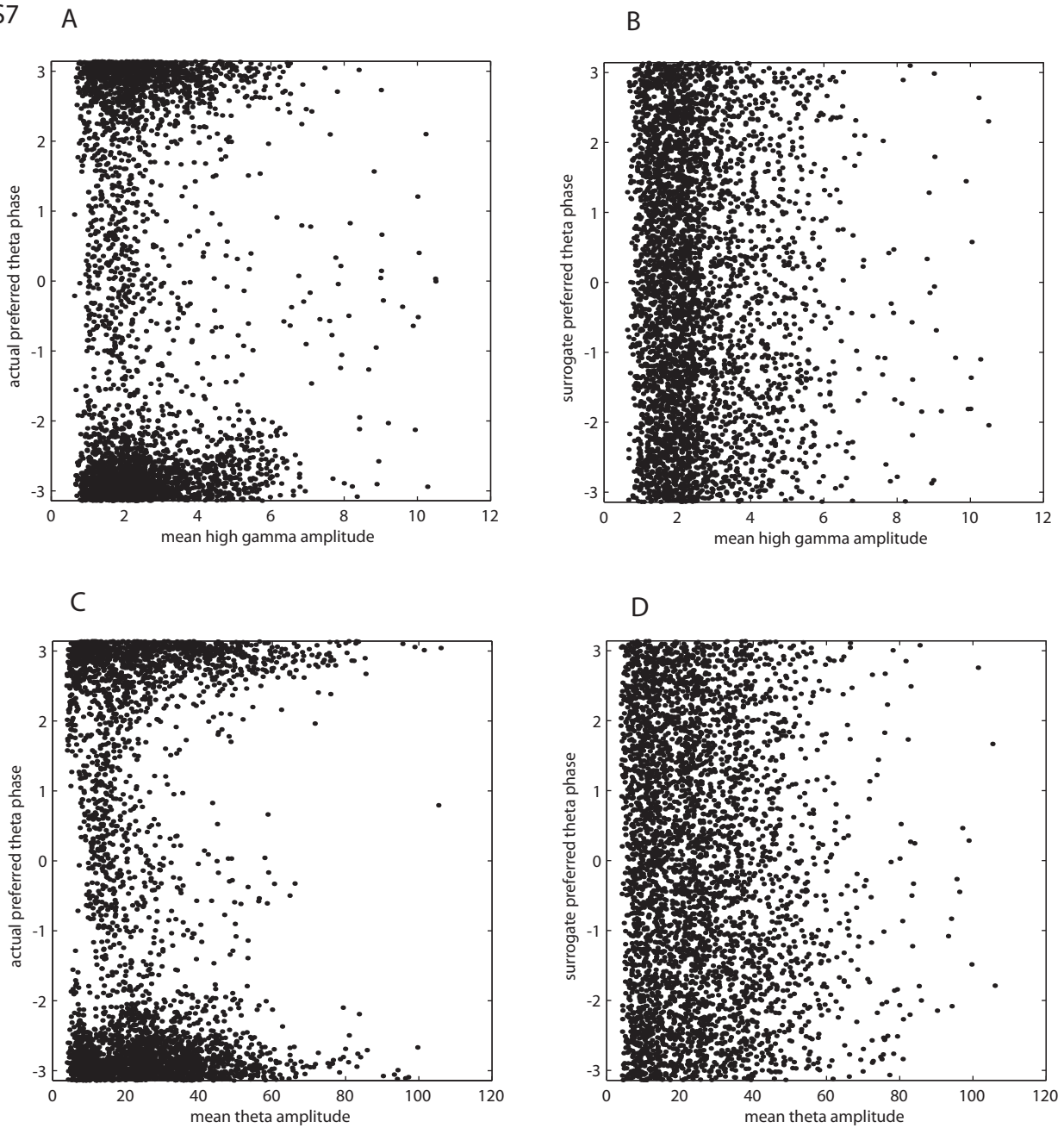
Fig. S7

FIGURE S7. LARGE HG AMPLITUDE VALUES OCCUR MORE OFTEN NEAR THE TROUGH OF THE THETA WAVEFORM.
A) Preferred theta phase as a function of mean HG amplitude for all actual modulation index values in all electrodes
in all subjects for all tasks. The theta trough corresponds to a postive or negative value of ?. B) Preferred theta phase
as a function of mean HG amplitude for all surrogate values in all data as above. Note that there is no dominant phase
as is the case for actual data. C) Actual referred theta phase as a function of mean theta amplitude for all data as above.
D) Surrogate preferred theta phase as a function of mean theta amplitude for all data as above.

FIG. S8.

THETA/HG COUPLING STRENGTH IS MAXIMAL
FOR SMALL LAGS BETWEEN THE TIME SERIES
BUT FALLS TO CHANCE FOR LARGE LAGS.
A) The modulation index as a function of the
time lag between the HG amplitude time
series and the theta phase time series for the
electrode analyzed in Fig. 1. The index has
been renormalized such that the maximal
value is unity. B) As in A, for all electrodes in
this subject which show significant coupling.
Electrodes have been sorted in order of the
lag producing maximal coupling. C) As in B,
for subject 2. D) As in B, for subject 3. E) As in B,
for subject 4. F) As in B, for subject 5
(same as Fig. 3A).
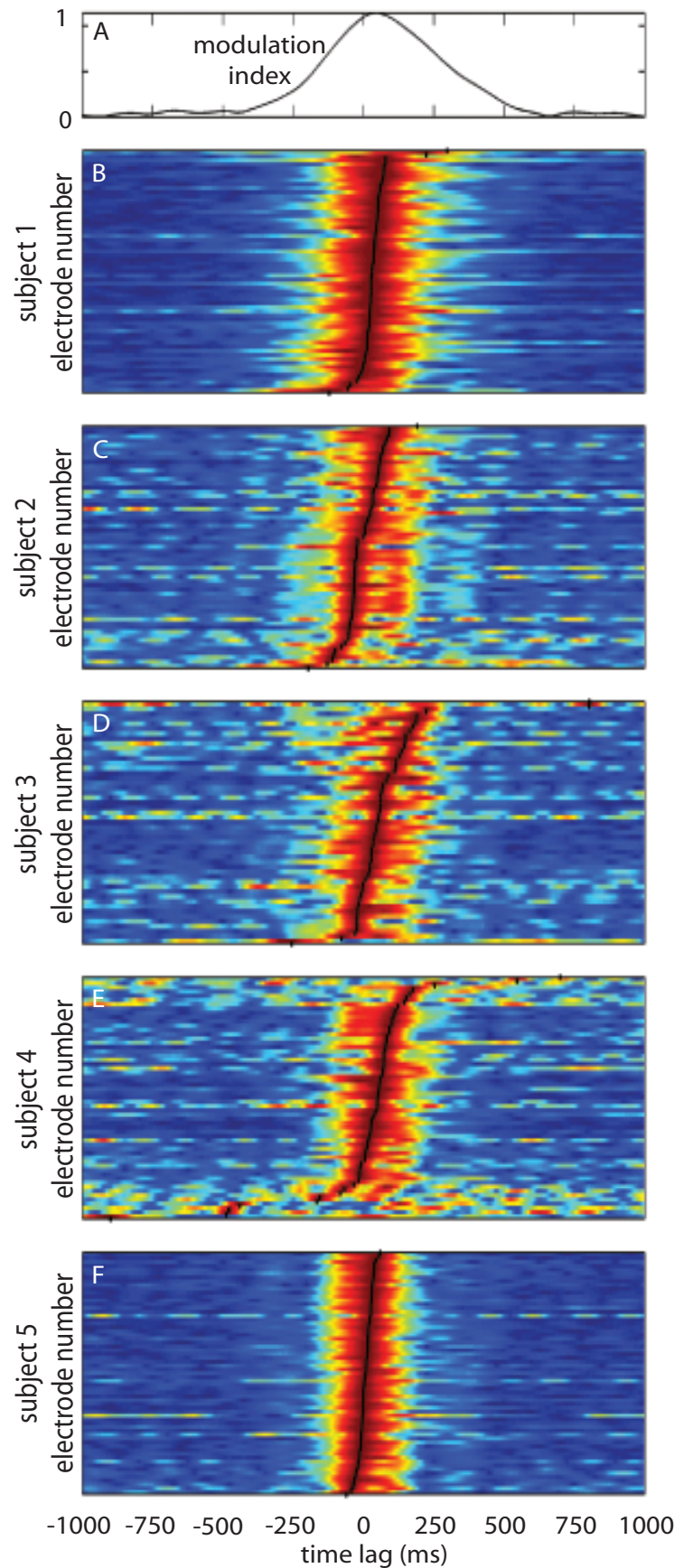
REFERENCES AND NOTES FOR SUPPORTING ONLINE MATERIAL

1.   A. Delorme, S. Makeig, *J. Neuro. Methods* **134**, 9 (Mar 15, 2004).
2.   N. E. Huang *et al.*, *Proc. R. Soc. Lond. A* **454**, 903 (Mar 8, 1998).
3.   Y. Benjamini, Y. Hochberg, *J. R. Stat. Soc. B* **57**, 289 (1995).
4.   G. J. Hahn, S. S. Shapiro, *Statistical Models in Engineering* (John Wiley & Sons, New York, 1994).